A REVIEW ON OPTICAL IMAGING

PREPARED BY:

SENIHA ESEN YUKSEL

CVIP Lab
University of Louisville
Electrical and Computer Engineering

Date: August 1, 2004

ABSTRACT

Optical imaging is the use of near infrared light to image the tissue. The use of NIR light is very beneficial as NIR is harmless and the optical properties of the tissue gives more accurate information on the tissue compared to the other techniques to image the tissue. But the drawback is the poor spatial resolution resolution because of the high scattering rate of NIR photons.

Optical imaging has branched into several techniques such as optical topography, optical coherence tomography, optical diffusion tomography and fluorescence optical diffusion tomography. These techniques are extensively discussed in this paper.

Optical topography gives 2D images. It is mostly used in functional imaging of infant brains.

Optical coherence tomography (OCT) gives images of the tissue microstructure by near-surface illumination. Although it has the penetration limit problem, OCT provides very high-resolution images and therefore preferred in areas like retinal diseases.

Optical diffusion tomography gives an image of the optical parameters of the tissues. These scattering and absorption parameters are reconstructed from boundary measurements of NIR photons. The reconstruction process is ill-posed and requires many iterations. Therefore many techniques have been introduced in literature to solve this problem. ODT has the deep tissue imaging capability, thus it has been used in many areas such as breast imaging, brain imaging and imaging of hemodynamics.

Fluorescence optical diffusion tomography (FODT) is an imaging technique which combines the deep tissue imaging capabilities of ODT with the high contrast and specifity properties of fluorescent dye tagging. FODT requires fluorophore to be injected into the tissue. Then the optical parameters and fluorophore parameters are both calculated from measurements in a way similar to ODT.

This paper gives a survey of these imaging techniques aiming to introduce the interested reader to the optical imaging area. The area is still open to contributions especially in the field of ODT and FODT as the derivation of the optical parameters is still a time-taking issue.

OPTICAL IMAGING

"Near Infrared light is a type of radio wave that has a little longer wavelength than that of visible light "

Optical imaging refers to the imaging techniques where near infrared (NIR) light is applied via optical fibers. It is used to obtain high-resolution spatial maps of functional properties from cortical areas, for cancer detection, for physiological monitoring and for many other applications which will be discussed in the later parts of this report.

Optical imaging is a very challenging technique in terms of extracting the optical information since biological tissue is highly scattering near infrared region which makes the algorithms complex. However, since optical spectra are directly related to the molecular conformation of biological tissues, optical imaging techniques are more sensitive to cancer detections and to physiological monitoring than other medical diagnostics [1][2]. They are also found to be popular since they don't necessitate such huge systems like in MRI imaging.

The advantages of optical imaging can shortly be listed as follows: [3]

i) Non-invasiveness through the use of safe, non-ionizing radiation,
ii) Display of contrast between soft tissues based on optical properties
iii) Disclosure of functional information, such as the oxygenation state of hemoglobin
iv) A facility for continuous bedside monitoring.

Optical imaging is a tool used in many sciences and has many techniques some of which are given below as definitions. These definitions are important to understand the history of optical imaging. However, the most popular optical imaging techniques, namely the optical topography, optical coherence tomography, optical diffusion tomography and fluorescence optical diffusion tomography will be explained in more detail.

- **Spectroscopy** is the use of the absorption, emission, or scattering of light to study the matter such as atoms, molecules. It has many versions such as atomic spectroscopy, electron, IR, laser, X-ray, gamma ray…

- **Raman spectroscopy** is a laser spectroscopy technique where the most common light source in is an Ar-ion laser. Raman spectroscopy is the measurement of the wavelength and intensity of inelastically scattered light from molecules. The Raman scattered light occurs at wavelengths that are shifted from the incident light by the energies of molecular vibrations. Because Raman scattering is a weak process, a key requirement to obtain Raman spectra is that the spectrometer provide a high rejection of scattered laser light [4]. Because of this complicated instrumentation for creation and detection of the weak optical signals, the technique is applicable mostly to in vitro experiments. The instrumentation for Raman spectroscopy is shown in Figure 1.

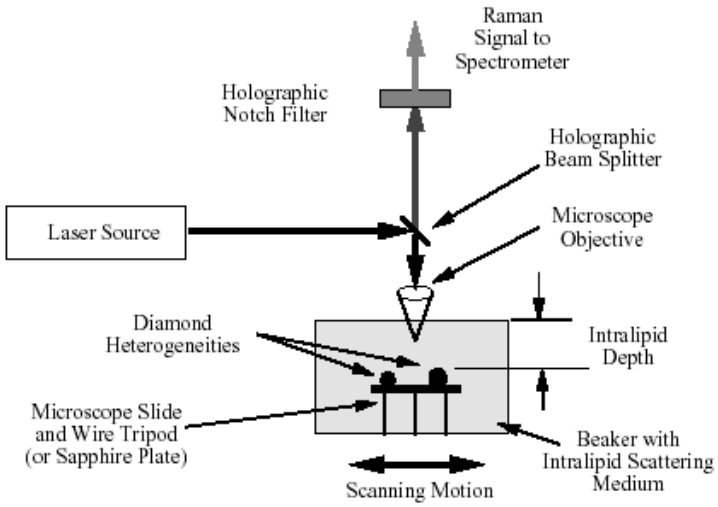

Figure 1: Raman Stereoscopy ([5])

- FLI stands for **Fluorescence Lifetime Imaging** where time or frequency resolved fluorescence is recorded and decay rate is represented as an image. In FLI, sources are applied at one wavelength and the resulting field excites a contrast agent to a metastable state which emits a second wavelength with time constant τ as a Poisson process. Information about tissue is taken from the lifetime of fluorescent[5]. The system for FLI Microscopy experiments is given in Figure 2.

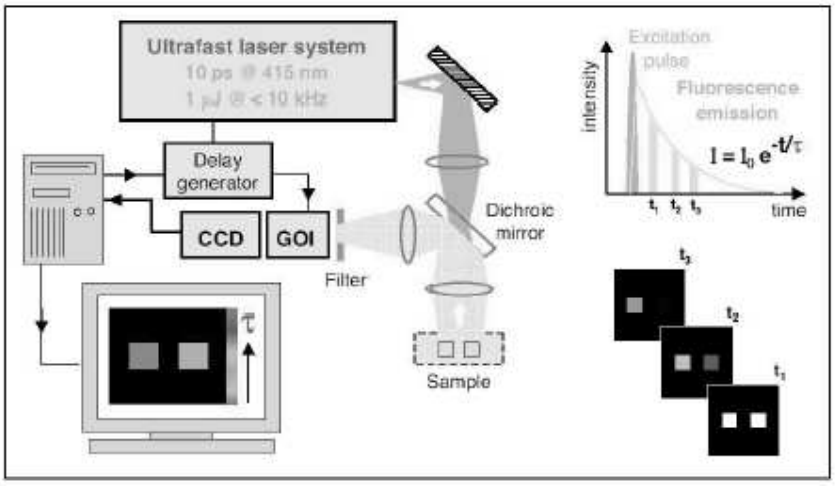

Figure 2: FLIM Experiment ([5])

In the following parts of this research, optical topography, optical coherence tomography, optical diffusion tomography and fluorescence optical tomography will be handled extensively.

OPTICAL TOPOGRAPHY

"Optical topography is a surface mapping technique which involves acquiring multiple measurements of diffuse reflectance at small source–detector separations over a large area of the head. By keeping the separation low, measured signals are relatively high and therefore may be acquired quickly, enabling fast hemodynamic changes within the outer (cortical) regions of the brain to be studied. Several groups have performed topography studies on infants in order to observe the cerebral homodynamic response to sensory stimuli"[6].

Study of young infants is critical to understand perceptual, motor, and cognitive processing in humans as it has been found that the pattern of hemodynamic response is qualitatively similar to the response observed in adults [7].

When a specific area of the brain is activated, the blood volume in that area increases to supply glucose and oxygen to the tissues as a result of the active metabolism. As a result the blood oxygenation parameters ([oxy-Hb] and [deoxy-Hb]) changes quickly. It can thus be determined where and how active the specific regions of the brain are, by continuously monitoring the blood hemoglobin levels, while having the examinee do some specific action [8]. Optical topography has been used especially on awake infants where blood oxygenation gives a clue, since brain imaging methods like Functional Magnetic Resonance Imaging (fMRI) and Positron Emission Tomography (PET) are difficult to apply on awake infants.

The system below has been developed by the Advanced Research Laboratory of Hitachi, Ltd. It uses near infrared light to measure the changes of oxy- and deoxy-hemoglobin as well as total blood volume changes in various regions of the brain's upper levels (cerebral cortex) [8].

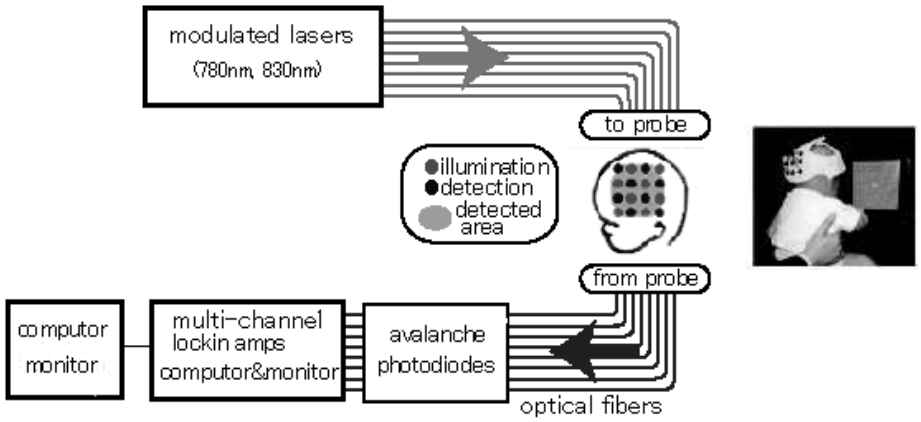

Figure 3: Optical topography system and how it is connected to the head ([7])

This system basically consists of a light source, a probe and a controller. The light source generates laser beam of 780nm and 830nm (for the two kinds of hemoglobin) through optical fibers. The probe directs the modulated laser light onto the examinee's head and receives the reflection back from the head. Reflected light is led to the photodiodes through the fibers. The controller converts the optical signals into the electrical ones, analyses the data and then displays the results.

"Weak near infrared light of about 1.5mW from a laser diode is illuminated onto head from optical fibers attached to the scalp. This light passes through the skull and reaches the cerebral cortex. It penetrates to a depth of about 30mm, and is scattered by hemoglobin in the blood. The light is partially reflected back through the scalp. The reflected light back on the scalp contains the information about the cerebral cortex and it is sent through optical fibers and received with a highly sensitive photodiode detector. The reflected light is measured every 0.1 seconds, and the latter measured data is subtracted from the former to determine the concentration change of hemoglobin."[8]

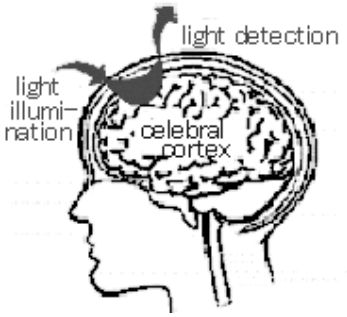

Figure 4: How OT works ([7])

The result is a colored contour map of the regions of brain which gives the name "topographic" to the method. The advantages of the method is its being safe using NIR light and the systems being small in size, allowing for continuous measurements and putting fewer restraints on examinee. Moreover, this system does not have the cross interference effect with the other modalities such as Electroencephalography (EEG) or MRI allowing the usage in combination with them.

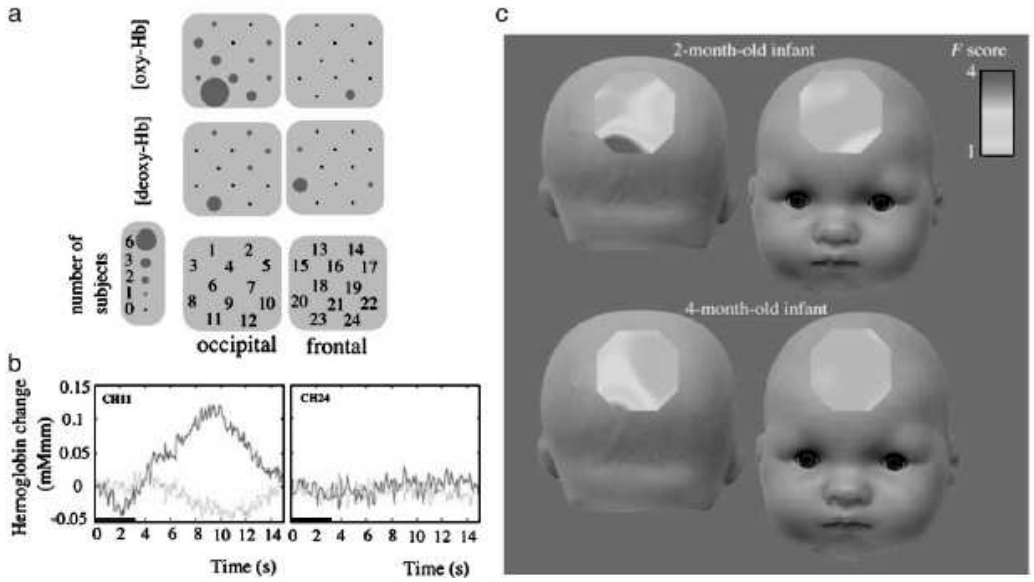

Figure 5: Optical Topography results ([8]) (a) Locations of significant changes in [oxy-Hb] and [deoxy-Hb] that were consistently observed among the subjects. The relative size of each red circle represents the number of the subjects who showed significant changes at the corresponding channel. For example, the largest circle at CH11 over the occipital cortex in [oxy-Hb] changes represents that six of the seven subjects showed significant changes in [oxy-Hb] at CH11. The channels illustrated with black dots indicate that none of the subjects showed a significant change. (*b*) Hemodynamic response of the occipital and frontal cortex averaged over all seven subjects. Shown are time courses of relative changes in [oxy-Hb] (red line) and [deoxy-Hb] (green line) at CH11 (*Left*) and CH24 (*Right*). (*c*) Topographic mappings of the activation of the occipital and frontal cortex in response to checkerboard pattern reversal stimulation for a 2-month-old (S1) and a 4-month-old (S6) infant. The color-coding topographic mapping was based on the spatial interpolation of *F* scores for the significant changes in [oxy-Hb] at 24 channels.

OPTICAL COHERENCE TOMOGRAPHY:

Optical coherence tomography (OCT) is an imaging modality to visualize tissue microstructure and to detect abnormal near-surface tissue. OCT relies on exposing a sample to a low coherence near-infrared light and then measuring the reflective response from different depths [9].

OCT technique was invented in 1991 by the Massachusetts Institute of Technology and the first commercial units became available in late 1996. It is used in the fields of gastroenterology, dermatology, cardiology, urology, orthopedics, gynecology, and ophthalmology.

OCT provides high-resolution, cross-sectional imaging similar to that of ultrasound, but it uses low coherence near-infrared light (around 800nm wavelength) instead of sound for better spatial resolution. In ultrasound sound waves are able to pass through tissue, whereas light, which has a much shorter wavelength, cannot penetrate beyond 2 mm in most non-transparent tissue. Apparently, the penetration limit is the disadvantage of OCT; however, the resolution (around 10μm) corresponds to an improvement of over 25 times that of high-frequency ultrasound, MRI or CT.

Another difference between ultrasound and OCT is the way they measure the delay time of sound/light. In ultrasound pulse propagation and detection is described in terms of time delays, but because of the high speed of the propagation of light, same techniques cannot be used for OCT to detect the echo delay time of light. Therefore, a technique known as Michelson interferometry is employed to get the depth of a tissue deformation.

Michelson interferometer is a device that allows one to use interference to determine the depth of a sample length when the wavelength is known. A free space interferometer is shown below:

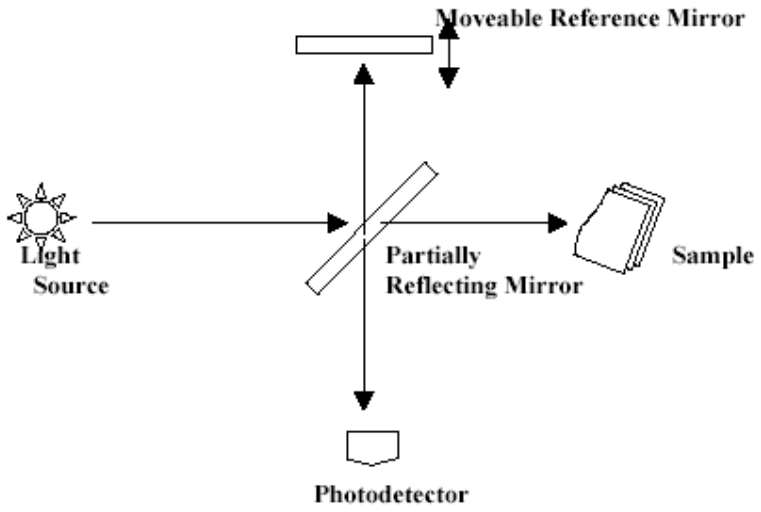

Figure 6: Diagram of a Free Space Michelson Interferometer ([10])

A low-coherence light source produces interference fringes only when integrated with light from the same source that has traveled the same distance. Michelson interferometer splits the source into two parts by a beam splitter and reflects the beams onto two different objects. When the beams combine back to form one beam again, they will produce an interference fringe pattern only if the distance they traveled is exactly the same. Hence, the interferometer determines if the two reflective objects were the same distance from the splitter or not.

Optical Coherence Tomography uses the Michelson Interferometer by some modifications. One of the split beams is made to be a controlled reference and the other is made to be the variable length scanning beam. The controlled beam is sent to a reference mirror whose position changes by micrometer increments. The other light beam is reflected from tissues according to their distance, thickness, and refractive index, and is then combined with the beam reflected from the moving reference mirror. When the path lengths of the two light beams coincide, an inference fringe is detected so the system can record the depth and the scattering parameters of the tissue at that point. A more detailed description of this system can be found in [9][10].

OCT techniques can be interfaced with optical fiber techniques to catheters, endoscopes, laparoscopes, and surgical probes to overcome the problem of penetration, allowing the method to be used deep inside the body. These attributes make it very attractive for medical and surgical diagnostics. It is a low-cost, portable technique and it allows the imaging of tissue structure at the micron scale in real time possibly replacing the conventional biopsy technique histopathology that requires removal of tissue specimens for microscopic examination. It also enables surgical guidance and imaging of organs while providing image resolutions one to two orders above conventional ultrasound [11]

OCT is mostly promising in the research areas of ophthalmology (the study of the eye) in monitoring the retinal diseases, tumors and age-related macular degeneration as shown in the figure below with the superior resolution compared to ultrasound. It is also useful in the diagnosis and monitoring of diseases such as glaucoma and macular edema linked to diabetic retinopathy and in vascular pathology, the study of how fluids, such as blood, travel through the body.

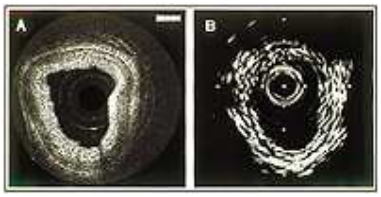

Figure 7: left: OCT image of human coronery artery , right: ultrasound.

OCT has better resolution

An Eye Clinic Example of Optical Coherence Tomography

Full Thickness **Lamellar**

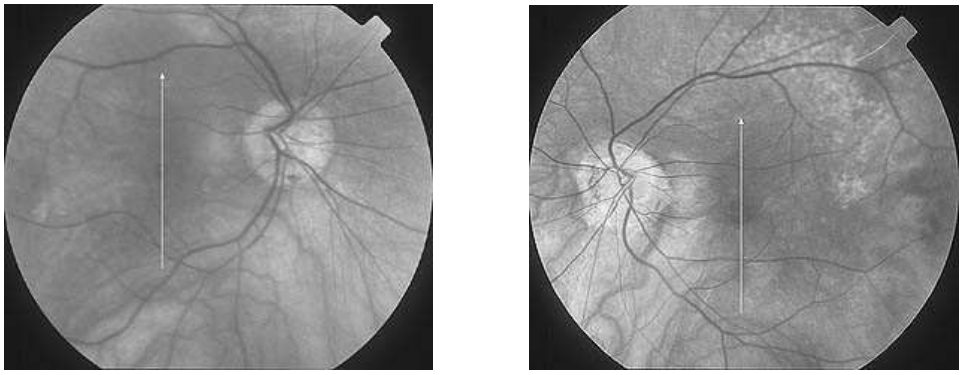

Fundus (bottom of the eye) images

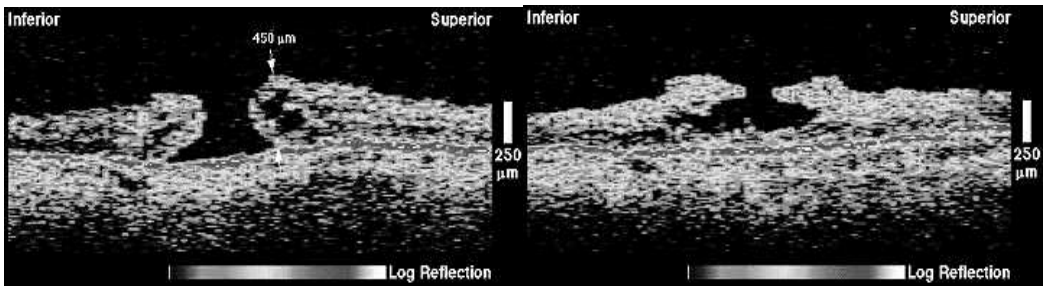

Figure 8: OCT images of a 69-year-old woman had a full-thickness macular hole in her right eye and a lamellar macular hole in the left. The fundus and OCT images of both eyes are displayed simultaneously [12].

OPTICAL DIFFUSION TOMOGRAPHY (ODT)

Optical tomography- also called Photon Migration Imaging (PMI) or Diffuse Photon Density Wave Imaging (DPDW)- is a low-cost, non-invasive, nonionizing, portable and fast imaging method which has the particular advantage of providing functional information.

In optical tomography systems, an array of sources illuminates the tissue by NIR light as in figure 9. This illuminating light can be sinusoidally modulated, continuous-wave or pulsed, where it undergoes multiple scattering and absorptions in the tissue before exiting. Then the scattered light is collected by an array of detectors and either intensity or phase information is measured. These boundary measurements from several sources are used to reconstruct 3-D maps of the absorption and scattering properties by optimizing a fit to diffusion models. The diffusion model is a partial differential equation, and it has nonlinear dependence on the unknown absorption and scattering coefficients. Therefore the inverse problem is computationally intensive and must be solved iteratively. The resulting image is composed of the spatially dependent absorption and scattering properties of the tissue. The contrast between the properties of diseased and healthy tissue might then be used in clinical diagnosis [13]. More mathematical information will be given on the ODT systems in the following sections after the discussion of the uses of this technology.

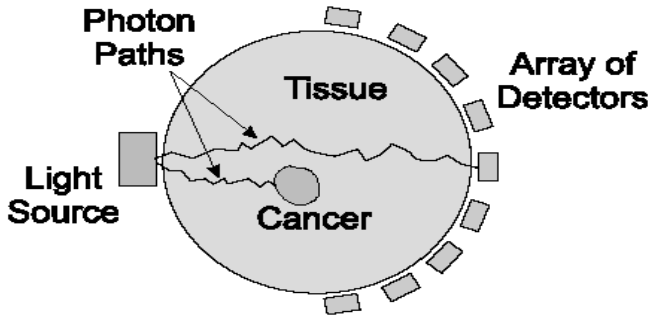

Figure 9: Optical diffusion tomograhy systems ([5])

There have been several systems developed for optical tomography for neonatal brain imaging, functional brain imaging, breast imaging for tumor detection and for the imaging of hemodynamics (ΔHbO_2, ΔHbT and ΔHbR).

In case of cancer or during cerebral activity, there is more blood going into the tissue to supply oxygen, showing absorption inhomogeneity. This change in absorption leads to the cancer detection and functional brain imaging via optical imaging methods [14]. Another good area is the study of strokes (condition due to the lack of oxygen to the brain which may lead to reversible or irreversible paralysis) and hemorrhage (the escape of blood from the vessels). Drugs can effectively treat ischemic strokes if identified in the first three hours. However, it is crucial not to use the drugs if the stroke is of hemorrhagic type, which would lead to rapid death. ODT can allow the early diagnosis and discrimination between ischemic and hemorrhagic strokes. Additionally, ODT is particularly useful if used as a bedside continuous monitor to provide real time information on the location and size of the bleeds in surgery. The currently used techniques such as EEG and fMRI are not as powerful in real time as ODT since EEG requires electrode

placements and fMRI is used for planning prior to surgery with complicated registration requirements [14].

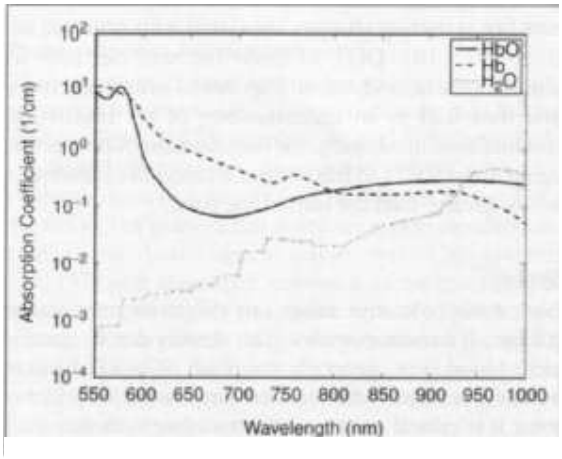

Figure 10: Hemoglobin and water absorption coefficients per mole as a function of wavelength

The three absorbers in the tissue – water, oxygenated and non-oxygenated hemoglobin – are relatively weak absorbers at the wavelengths of NIR light.

At higher frequencies however, the absorption of the water increases rapidly prohibiting the use of this method. Within this window of wavelengths, the spectra of oxy and deoxy-hemoglobin are distinct enough to offer the possibility of performing spectroscopy: illuminating several wavelengths and recovering separate concentrations of both types of molecules which gives the opportunity to image 3D spatial variations in blood parameters[13]

ODT instrumentation doesn't need coherent light (inexpensive), it uses NIR light (no radioactive exposure), and it achieves faster frame rates compared to PET or MRI. However, ODT needs a high resolution to separate the tissues and it doesn't have the resolution of CT or MRI. It has approximately 1mm spatial resolution, temporal resolution of up to 1 ms and it can go 1-10cm deep in tissue. Because of this depth limitation, the method is especially used for infant brain and breast applications.

"ODT complements PET, fMRI and EEG. PET directly images changes in metabolic activity, but has poor temporal and spatial resolution. fMRI images blood flow and the concentration of deoxy-hemoglobin with high spatial resolution and good temporal resolution but cannot also simultaneously measure oxy-hemoglobin concentration. EEG and MEG monitor neural activity with much better temporal resolution (100 to 1kHz), but localization of the origin of electrical and magnetic sources is difficult and spatial resolution is poor compared to fMRI. With ODT, although its spatial resolution is inferior to fMRI, it is possible to simultaneously measure concentrations of oxy and deoxy-hemoglobin as well as blood volume with good temporal resolution, as well as to potentially measure fast scattering changes associated with neural activity" [13].

Again, as with all the optical systems, the main problem is the tissue being a highly scattering environment causing the photons travel in irregular paths (shown in figure 12). Therefore not only the reconstruction but also the collection of data is a big challenge and a basic matrix inversion as in X-ray imaging cannot be employed. In the following sections, technical issues – formulas & derivations – will be discussed and some current applications of ODT will be given to show the existing systems and the results.

TECHNICAL KNOWLEDGE BEHIND ODT

A volumetric image can be formed using surface measurements of the scattered light that has passed through the tissue. The task of ODT is to take these surface measurements and to form the image from them. The formed image will carry the information about the absorption and scattering properties of the tissue, analysis of which will help to detect diseases such as cancer.

How to use these measures of light to recover the parameters of interest and form an image is a two fold problem. The first problem is called the forward problem. In the **forward problem**, the propagation of light in tissue is modeled by the use of partial differential equations (PDE). In the **inverse problem**, the reconstruction of the optical parameters thus the reconstruction of the image is handled using the model of the forward problem, a model for the noise, some boundary conditions and the actual measurements. A definition and a basic shematic for the forward and inverse problems can be given as follows:

*Forward problem: "Given a distribution of light sources {**q**} on the boundary ∂Ω of an object Ω, and a distribution of tissue parameters {**p**} within Ω, find the resulting measurement set {**y**} on ∂Ω.*" [15]

*Inverse Problem: "Given a distribution of light sources {**p**} and a distribution of measurements {**y**} on ∂Ω, derive the tissue parameter distribution {**p**} within Ω.*" [15]

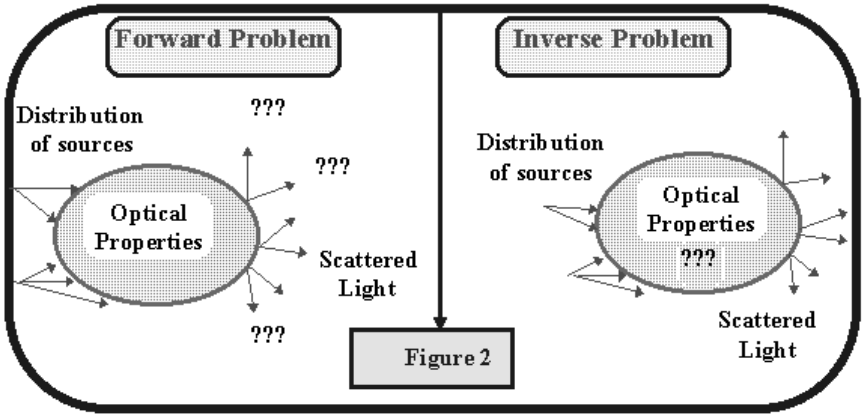

Figure 11: Forward an Inverse Problems in ODT ([16])

Forward Modeling:

The **forward problem** is how to interpret the propagation of light in tissue. To interpret the propagation, a model of the propagation of light in tissue is developed and parameterized in terms of the unknown scattering and absorption parameters as a function of position in the tissue. There are several common models used that involve either the assumption of particle or wave phenomenon for the propagation of light. For the wave assumption, diffusion models are commonly used. For the particle assumption, transport models or Monte Carlo methods have been employed in the literature.

The model used for the forward problem depends on the type of the system being used. Optical tomography systems can be divided into 3 groups: constant wave illumination, frequency domain and time domain systems. The photon flux density obeys the time domain diffusion equation in time domain systems or the elliptic PDE in frequency domain systems. The advantages and disadvantages of the type of systems are given below.

Types of the systems:

The constant illumination technique, called **Continuous Wave (CW) illumination** (also called as DC systems), is the easiest method to collect data of the photon migration. In this method, the tissue is illuminated by a continuous source of light and the amplitude decay (transmitted intensity) of the light at the surface is measured. DC systems are popular to detect changes in absorption for example between resting and activated tissues, or between measurements with and without a contrast agent. However, the general problem of optical imaging is to reconstruct the absorption and scattering parameters. Since the measured quantity is only the intensity, DC measurements suffer from non-uniqueness in the possible reconstructions, which lead to an inability to unambiguously separate absorption from scatter. Therefore, generally, time domain and RF amplitude modulated frequency domain techniques are employed [13], [17].

In **time-domain** systems, the applied illumination is an ultra-short input pulse and measured quantity is the temporal distribution of the photons as they leave the tissue, which gives the histogram of photon time-of-flight. A basic figure of time domain imaging is given in figure 12. In time domain imaging, the early arriving light from a short pulse is measured with one of the methods for time gating. But due to the high scattering, few direct-path photons can be measured, therefore the first arriving photons are assumed to have traveled a direct length. To be able recover early arriving photons, the distance between the source and the detectors should be small. Since the SNR of the measurements is related to the number of photons arriving in a measurement interval, time domain methods have a low SNR problem. The advantage of time domain systems is the path length information and the better performance in the lowest photon count region when relatively large bodies are being imaged. However, time domain systems are more expensive as they need to compute an extra dimension – time.

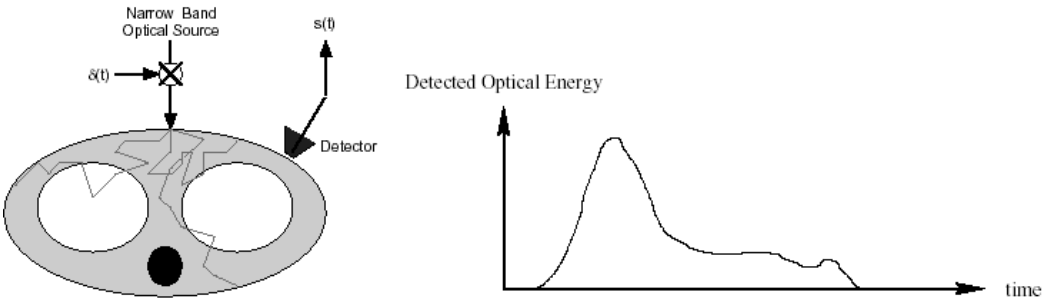

Figure 12: Time domain measurements -- based on the distance traveled due to scattering ([5])

In **frequency-domain** systems, the applied illumination is amplitude (intensity) modulated and the measured quantities are the amplitude and phase of the modulated light envelope. Information about the absorption and scattering properties of tissue are obtained by recording amplitude decay and phase shift of the detected signal with respect to the incident one. RF amplitude modulated frequency-domain systems are attractive due to their relatively low cost of construction, and the requirement in the modeling of the system to solve a single complex elliptic equation [13],[16][17]. A basic figure of frequency domain imaging is given in figure 13.

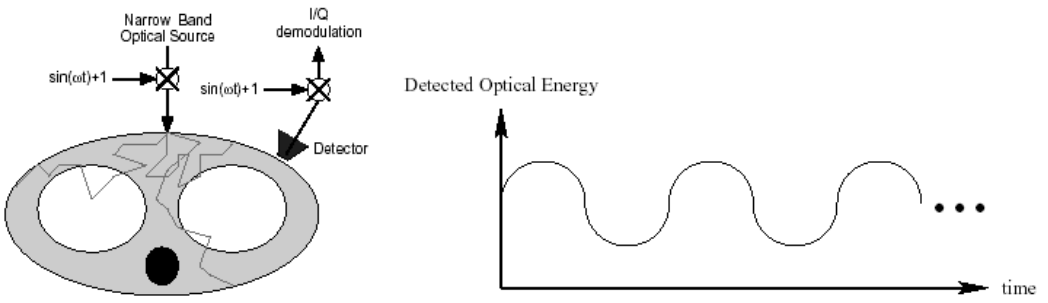

Figure 13: Frequency domain measurements -- based on the change in magnitude and phase of detected signal due to scatter and absorption ([5])

Models of light:

Turning back to the modeling problem, the propagation of light has in general been modeled by Maxwell's equations. However, this model is not feasible when interactions are very large between photons as in turbid media like tissue. In the coming sections three stochastic models -- Monte Carlo, Random Walk, and Markov random field models – and two deterministic models -- radiative transport equation and photon diffusion equation – will be discussed.

Stochastic Models:

In **Monte Carlo** methods, photons are treated as distinct particles with a certain probability of scattering and absorption at every point in a discrete geometry. Photons are injected into the medium at every source and they are followed until absorbed or escape the surface, thus contributing to a measurement. Such methods offer great flexibility in modeling arbitrarily complex geometries and parameter distributions, but they are prohibitively costly in computational time. For tissue thicknesses of several centimeters, typical photon paths are several hundred interactions in length, and many millions of photons need to be followed to obtain useful statistics [13] and[15].

"**Random walk theory** (RWT) describes the statistical behavior of random walks in space, constrained along the elements of a discrete lattice. Although working within a simple structure, such as a cubic lattice, severely restricts the number of directions in which motion is possible, a powerful description of photon migration is achieved using a relatively simple mathematical analysis. When motion in a homogenous space occurs with each of the lattice directions having equal probability, RWT can be considered to be equivalent to a finite difference approximation of the diffusion equation."[15]

"The **Markov random field** method is a stochastic model based on transition probabilities. The model can recover the internal transition probabilities in the time independent case given exact values of the probabilities on the boundary of a domain. Thus the model expects noiseless data. Despite leading to an exact solution to the non-linear inverse problem it has never been applied to real data because of the difficulty in relating the essentially topologically invariant analysis to real conditions."[15]

Deterministic models:

The radiative transport and photon diffusion equations and their solution methods will be given in this section**.**

Radiative Transport Equation:

Since the interactions are very large between photons in tissue, it is convenient to model them as particles i.e. photons, rather than as waves. The linear transport theory takes the light as a composition of distinct particles, propagating through a medium modeled as a background which has constant or variable scattering and absorption characteristics, possibly containing discrete, bounded regions of absorption and scattering inhomogeneity [13]. This model brings the conservation of radiance equation, also known as the **radiative transport** or Boltzmann transport equation. **Boltzmann equation** is known as:

$$\frac{1}{\nu}\frac{\partial L(r,\hat{\Omega},t)}{\partial t}+\nabla.L(r,\hat{\Omega},t)\hat{\Omega}+\mu_t L(r,\hat{\Omega},t)=\mu_s\int_{4\pi} f\ (\hat{\Omega},\hat{\Omega}')L(r,\hat{\Omega}',t)d\hat{\Omega}'+Q(r,\hat{\Omega}',t)$$

where
L(r,Ω,t): radiance (the power per unit area) at position r in the direction of Ω at time t.
$\mu_t = \mu_s + \mu_a$: optical transport, scattering and absorption coefficients.
υ: electromagnetic propagation speed in the medium
f (Ω, Ω'): scattering phase function
Q (r, Ω, t): radiant source function

This equation can be stated in words as follows:[13]

$$\begin{bmatrix}net\ \#of\\ photons\\ entering\\ the\ element\end{bmatrix}+\begin{bmatrix}flux\ of\\ photons\\ along\\ direction\ \Omega\end{bmatrix}+\begin{bmatrix}scattering\ \&absorbtion\\ of\ \ photons\ within\\ the\ phase\ element\end{bmatrix}=\begin{bmatrix}photons\ at\ \ position\ r\\ being\ scattered\\ from\ all\ directions\\ \Omega'\ into\ \ \Omega\end{bmatrix}+\begin{bmatrix}photon\\ source\end{bmatrix}$$

So the left hand side accounts for photons leaving the small volume element around position r in the direction Ω at time t, and the right hand side accounts for photons entering it.

"The Boltzmann transport equation describes the photon transport in the presence of scattering. However, analytical solutions are available only for simple scenarios because of the integro-differential structure of the equation and numerical solutions are computationally expensive due to the dependence on space, angle and time." [13]

Photon Diffusion Equation:

If the medium is strongly scattering, i.e. the scattering probability is much larger than the absorption, Boltzmann transport equation reduces to the **diffusion equation**. Since NIR light is strongly scattered inside most biological tissues, the diffusion equation has been widely employed in optical tomography studies.

In highly scattering tissue, in **time domain**, the photon flux density obeys the diffusion equation below:

$$\frac{1}{c}\frac{\partial}{\partial t}\psi(r,t)-\nabla\cdot D(r)\nabla\psi(r,t)+\mu(r)\psi(r,t)=S(r,t)$$

where

ψ(r,t): photon flux density (photon per unit volume)
$D(r)=\frac{1}{3(\mu(r)+\mu_s'(r))}$ = diffusion coefficient (cm)
μ(r) = absorption coefficient (cm^{-1})
S(r,t) = instantaneous power density of source at location r and time t
r,t : 3D position and time

In **frequency domain**, if the source is modulated by e^{jwt}, then the frequency modulated light $\phi(r)$ obeys the elliptic partial differential equation:

$$\nabla \cdot D(r)\nabla\phi(r) - [\mu(r) + j\omega/c]\,\phi(r) = -S(r)$$

where $\psi(r,t) = \phi(r)\, e^{j\omega t}$ and $S(r,t) = S(r)\, e^{j\omega t}$

Actually, this equation is nothing but the **Helmholtz equation**:

$$\left[\nabla^2 + k^2\right]\Phi(r,\omega) = \frac{-\nu}{D} S(r,\omega)$$

where k is the complex wave number $k^2 = \frac{-\nu\mu_a + j\,\omega}{D} = 3\mu_s^{'}(-\mu_a + j\,\frac{\omega}{\nu})$

and photon density = $\Phi(r,t) = \int_{\Omega^{n-1}} \phi(r,\Omega,t)\, d\,\Omega$

How to solve the deterministic models:

In all these methods described above, the main objective is to measure the light $\phi(r)$ and to reconstruct the optical parameters $\mu(r)$ and D(r) by solving the forward models.

To solve the deterministic models, first, some boundary conditions should be found. Then, analytical methods or numerical approximations should be applied to solve the equations.

Analytical solutions:

One analytic solution to the time domain diffusion equation is the Green's function:

$$G(r, r', t, t') = \frac{e^{-\mu_a t - \frac{|r-r'|^2}{4D(t-t')}}}{(4\pi D t)^{3/2}} \qquad t > t'$$

The Green function is the solution when the source is a δ-function. But using it is still appropriate for the case of pulsed sources, since the pulsed sources in optical imaging are often sufficiently close approximations to δ-functions. Green functions have been published for various homogeneous geometries (slabs, cylinders and spheres), for both the time and frequency domains.

However, Green's function works only in some certain restricted geometrics. In the presence of arbitrary boundaries and heterogeneous distributions of parameters $\mu_a(r)$ and D(r), the Green's function is not known so the diffusion equation should be solved by numerical techniques. Moreover, analytical solutions for the radiative transport equation are scarce and have been obtained for only very simple cases like the one-dimensional geometries [15][17].

Numerical solutions:

"The commonly applied numerical approximations to the partial differential equations are the finite difference, finite element or truncated series approximations based on perturbative approaches such as the Born and Ryton or the extensions of these methods. These methods depend on modeling the fields in the medium as a superposition of incident and scattered waves." [13]

In general, the perturbation method is stated as follows: [15]
Let the question to be solved be y=F[p]. If we have an estimate $\hat{p}$ that is close to the ideal solution, then its projection $\hat{y} = F[\hat{p}]$ is close to ***y***. We can expand equation y = F (p(r)) in a Taylor series

$$y = F[\hat{p}] + F'[\hat{p}](p - \hat{p}) + (p - \hat{p})^T F''[\hat{p}](p - \hat{p})$$

where ***F'*** and ***F''*** are the first- and second-order Frechet derivatives respectively. In the discrete case, these derivatives are over a finite number of dimensions and are represented by matrices $F' \to J$, the Jacobian and $F'' \to H$, the Hessian. Putting $\Delta y = (y - \hat{y})$ *and* $\Delta p = (p - \hat{p})$ leads to the solution

$$\Delta y = J[\hat{p}]\Delta p + \Delta p^T H[\hat{p}]\Delta p + \ldots$$

"According to this solution, in the perturbative methods the signal reaching the detector is considered to be superposition of the diffuse photon density waves (DPDW) that traveled through a homogeneous system plus the first order scattering waves from the optical inhomogeneties and so on. The optical properties of the background are usually taken to be the average or most common optical properties. For computational purposes, one generally divides the region of interest into voxels, and the first order scattered DPDW is then the scattering of the incident DPDW from each voxel. The voxels are chosen to be small enough so that the scattered DPDW can be linearized, and the amplitude of the scattered wave is then assumed to be linearly proportional to the change in μ_a and μ_s'. Using only this first order term gives the Born or Rytov approximations."[13] The two methods, finite difference and finite element, that use this technique is explained below.

"The finite-difference method (FDM) is a standard technique to solve a PDE. A regular grid is established in the problem domain and differential operators are replaced by discrete differences. Then the problem becomes sparse matrix algebra. For elliptic equations (frequency-domain DE) the multi-grid scheme has been found to be optimal and it has been applied in optical tomography. For parabolic equations (time domain DE) the alternating direction implicit scheme has been found to be optimal, provided that the grid is regularly spaced in each direction. The FDM can also solve the transport equation, provided that the angular integral over scattering directions is discretized."[15]

"The finite-element method (FEM) is somewhat more versatile than the FDM, especially in regard to complex geometries and for modeling boundary effects. The key principle in the FEM as applied to photon transport problems is the reduction of the general problem to that of finding an approximate solution that lies in the vector space spanned by a finite number of basis functions. Then the forward problem is reduced to one of matrix algebra of a finite size for which efficient techniques have been developed. In principle this method can be applied to any PDE model of the transport process."0[15] and [17]

Inverse Problems -- Image Reconstruction:

The formation of an image representing one or more internal optical characteristics from a series of boundary measurements is an example of a so-called inverse problem. The inverse problem is nonlinear, ill-posed and generally underdetermined. Ill-posed means that the relatively large changes in the parameters of interest tend to result in relatively small changes in the measurements. Thus inverse solutions must amplify these small differences; as a consequence measurement noise and model error will be amplified as well, causing inverse solutions to be erratic. So the problem should be constrained by additional a priori knowledge or assumptions. Therefore unique and reliable solutions are hard to find, thus several tools like regularization, optimization, statistical modeling or parametric representations are employed to obtain stable results [13]. Statistical models such as the Bayesian maximum a posteriori (MAP) solution help to deal with the different types of noise. Parametrical models serve to reduce the under-determinedness and ill-posedness of the problem [14].

Regularization helps to stabilize the inversion of the forward model by adding a second term to be minimized to the least squares fit of the estimate to the data. For example if we want to estimate the absorption coefficient $\mu_a(r)$, using fluence measurement y and forward model $h(\mu_a)$, the following equation should be solved where λ is the regularization parameter and R is the norm. The second term in the equation is used to put some constraints on the solution.

$$\hat{\mu}_a = \text{argmin}_{\mu_a} \|y - h(\mu_a)\|_2^2 + \lambda^2 R(\mu_a)$$

The regulation formulations can be solved by a variety of optimization methods. The major issues in selecting the optimization methods are the per iteration computations, number of iterations to converge, enforcement of convex constraints, convergence to local and global minimum and the ease to do parallel implementation. Of the linear/nonlinear/multigrid optimization techniques, there has been several choices like the gradient descent, steepest descent, conjugate gradient, Gauss-Seidel, Levenburg-Marquardt methods as well as wavelet based and multigrid approaches. For more information on the optimization techniques, the reader is encouraged to look at the tutorial by Bouman *et al.* [5].

Another method for image reconstruction is the **perturbation method**. In the perturbation formulation given in the previous section, if the terms after the first are neglected, the problem becomes linear and the problem reduces to inversion of the matrix representation of **J** at $\hat{p}$. Applying this perturbation method to our problem, the term $h(\mu_a)$ in the regularization equation given above can be approximated as a matrix, $h(\mu_a) = H \mu_a$. This linear problem may be ill posed, and is amenable to standard matrix inversion methods. Its success is largely dependent on how closely the initial estimate is to the correct solution, and how little effect is played by higher-order terms in equation. Therefore, for the solution of this linear approach, a variety of methods has been reported. The direct methods include singular value decomposition (SVD), truncated singular value decomposition (TSDV); the indirect methods include algebraic reconstruction techniques (ART), simultaneous iterative reconstruction technique (SIRT) and conjugate gradient methods like the truncated conjugate gradient (TCG).

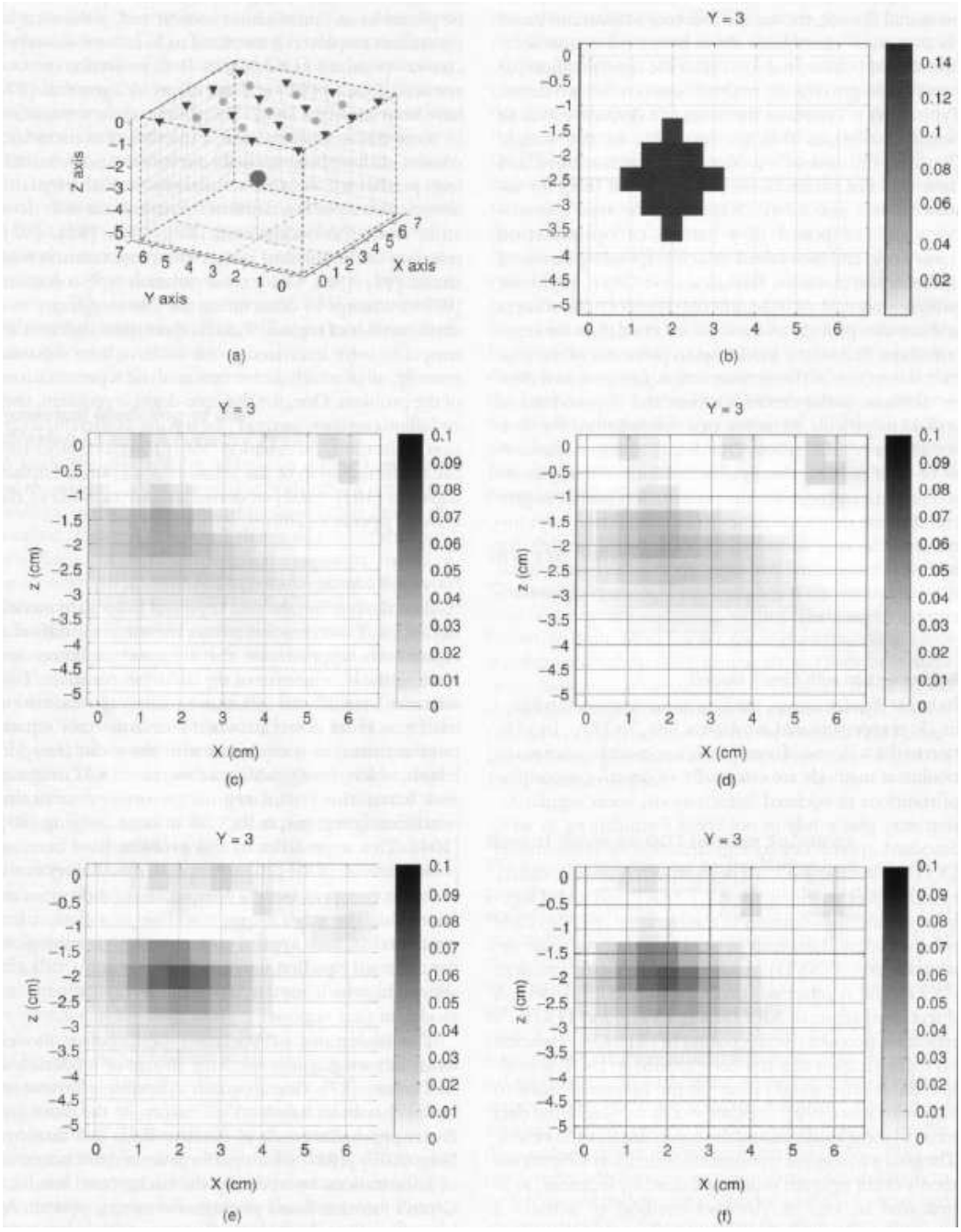

Figure 14: Reconstruction example for four linear reconstruction techniques at 20dB SNR. A) volume with inhomogeneity B) Vertical slice through the center of the true image C) ART algorithm D) SIRT algorithm E) TSDV algorithm F) TCG algorithm [13]

Some Applications & Systems of ODT:

Three applications of diffuse optical tomography will be given in this part to show the existing technologies and to familiarize the reader with the results of these applications.

1) Neonatal Imaging: *(Time domain ODT system example)* [3],[6],[8]

Optical tomography of the neonatal brain is used to help doctors diagnose and treat newborn babies suffering from hypoxic-ischemic brain injury. This occurs when breathing difficulties prevent the baby from receiving sufficient amounts of oxygenated blood during birth and it is major cause of permanent disability in preterm infants.

The optical tomography system shown in figure 14 was developed in 1999 at The Biomedical Optics Research Laboratory at University College London. It acquires three-dimensional (3D) images of the infant brain which reveal the variation in blood volume and tissue oxygenation.

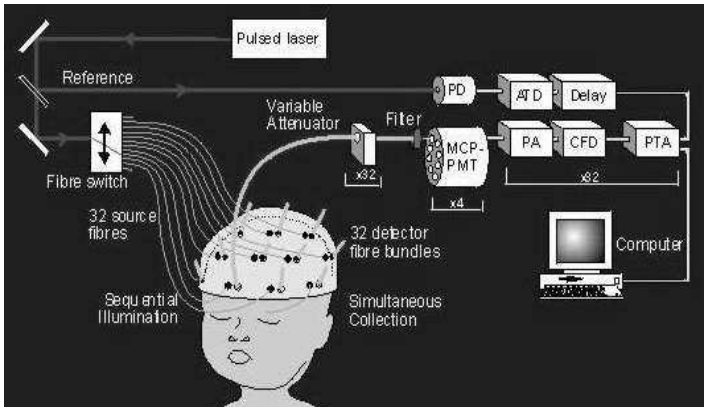

Figure 15: ODT System for Neonatal Imaging ([3])

The source/detector fiber bundles are arranged over the surface of the neonatal head. Pulses of light from a fiber laser are coupled into a series of optical fibers. The point of illumination on the tissue surface is varied sequentially. Then the transmitted light is collected by fiber detector bundles. Electronic pulses generated each time a photon is detected are sampled by an electronic system. By measuring the delay between these pulses and a reference signal received directly via the laser, histograms of photon flight times are recorded.

Figure 16 shows transverse, coronal, and sagittal views across the 3D reconstruction of the absorption coefficient at a wavelength of 780 nm. The coronal image exhibits greater absorption on the left side of the brain, consistent with the larger intraventricular hemorrhage. The transverse and sagittal images are dominated by a feature at the rear of the head, possibly due to the proximity of the sagittal sinus, since it represents a dominant source of venous blood close to the surface.

Figure 16: An ultrasound scan of an infant brain revealing a large haemorrhage in the left ventricle ([3]).

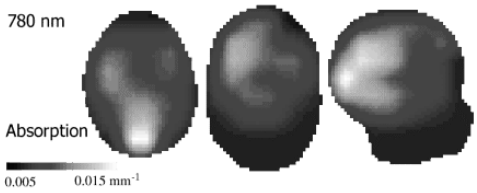

Figure 17: Transverse, coronal, and sagittal views across the 3D absorption image of the infant, acquired at 780nm. ([3]).

2) Breast Imaging:

Two example systems are given below for breast imaging systems. The first system uses time domain techniques as in the neonatal imaging, whereas the second one employs frequency domain techniques.

a) Time Domain ODT System for Breast

The standard diagnostic tool for breast imaging is x-ray mammography but it suffers from harmful ionising radiation, and a large number of false positives leading to unnecessary biopsy. Therefore, ODT offers several major advantages over the existing techniques since it uses non-ionizing radiation, it doesn't require compression and it also gives functional parameters as well as the structural differences. Moreover, if allows the simultaneous reconstruction of the entire three-dimensional volume of the breast[3].

Figure 19: Source and detector fibres attached to three rings mounted on a conical phantom ([3])

Figure 18: Fibre holder rings and support frame for optical tomography of the breast ([3])

Results:

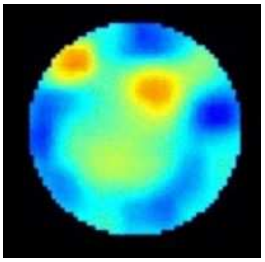

Figure 20: A breast image exhibiting a fibroadenoma at top left ([3])

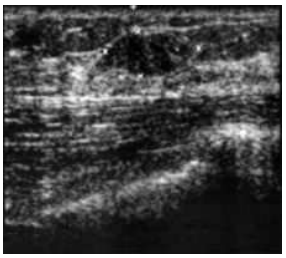

Figure 21: An ultrasound image of the same fibroadenoma (top centre) shown in figure 16 ([3]).

b) Frequency Domain ODT System for Breast

Another breast cancer detection system has been implemented by the Dartmouth College [18]. The system shown in Figure 21 uses frequency domain techniques for optical tomography. This device employs radio-frequency intensity modulated near infrared light to image quantitatively both the scattering and absorption coefficients of tissue. The functioning components of the system include a laser diode and a photomultiplier tube, which are multiplexed automatically through 32 large core fiber optic bundles using high precision linear translation stages. Image reconstruction is based on a finite element solution of the diffusion equation.

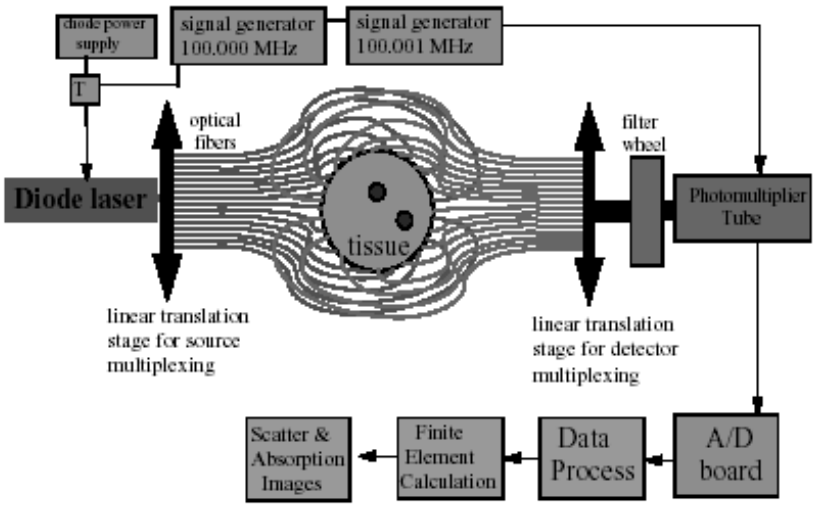

Figure 22: Frequency Domain ODT System ([18])

3) Functional Imaging:

In the functional imaging systems, the aim is to measure the changes in oxyhemoglobin ([HbO2]), deoxyhemoglobin ([HbR]) and total hemoglobin ([HbT]=[HbR]+ [HbO2]) concentrations in response to cortical activation. Unlike fMRI, ODT can directly and simultaneously measure concentration changes allowing the real-time observation of the hemodynamic response. Moreover, ODT is superior to fMRI in the sense that it can measure the HbO2 concentration. Since HbO2 is diamagnetic, it has minimal influence on proton precession and thus cannot be measured with fMRI. Also, ODT makes the measurements at multiple source wavelengths so the changes in the three kinds of concentrations can be calculated independently.

"But ODT also has some limitations too. As the image reconstruction process is ill-posed, it can lead to errors in the hemodynamic characterization. Also, features with high absorbance, such as large blood vessels, can absorb nearly all of the local incident flux, thus reducing DOT signal sensitivity in these areas. Thus, most DOT measurements are uniformly sensitive to vessels smaller than the optical absorption length, with sensitivity progressively decreasing for larger vessels."[19]

The following studies show the systems where functional imaging has been done using ODT. The first study below is on rats and the second study is on human brains.

a) Hemodynamics in Rats: (Continuous-Wave ODT system)[19]

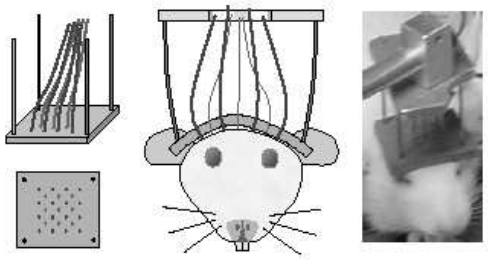

Figure 23: Functional imaging in rats([19])

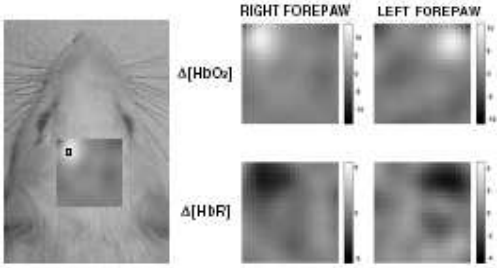

Figure 24: The ODT image([19])

In this system, the data is collected via 9 pairs of collocated dual-wavelength (690 nm and 830 nm) fibre-coupled laser diode sources and 16 fibre-coupled silicon APD detectors. For image reconstructions of spatially varying optical properties, a standard linear approach known as the Rytov approximation is employed. Then the integral is discretized into cubic voxels (*h*3) and the Rytov approximation is applied using the Green's function of the photon diffusion equation for given background optical properties, and a semiinfinite geometry with extrapolated zero boundary conditions. Then the inverse problem is then solved using the (Tikhonov regularized) Moore–Penrose Generalized Inverse. The result is the concentration changes vs. time as seen in figure 24.

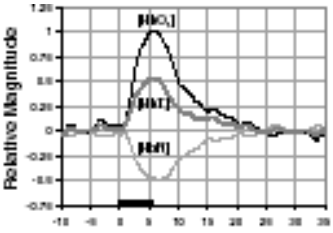

Figure 25: Hemodynamics in rats

b) 3D Hemodynamics in Humans:

The first study on the volumetric reconstructions of the optical properties in human head was published by Hielscher *et al* [20]. This study uses a three dimensional, continues wave diffusion equation with the Robin boundary conditions. Then the equation is solved numerically using a finite element method. For the finite element forward model, the domain Ω is divided into *P* elements, joined at *N* vertex nodes. The solution is approximated by a piecewise linear function spanned by a set of linear basis functions φ. The solution is obtained by sparse matrix inversion using the preconditioned conjugate gradient method The discretized forward model can be written as $A\varphi_c = S$ where A is the finite element stiffness matrix of the diffusion equation forward model. Each element of the tetrahedral mesh, with nodes i, j has a corresponding 4×4 A^e element stiffness matrix with entries defined by

$$A^e_{i,j} = \int D\nabla\varphi_i \nabla\varphi_j + \mu_a \varphi_i \varphi_j \, d\Omega_e$$

where the diffusion coefficient D = 1/ 3(μ_a+μ_s') , μ_a is the absorption coefficient, and μ_s' is the reduced scattering coefficient.

To find the coefficients μ_a and μ_s, an initial guess is made (ξ_0 = (μ_a = 0.1cm^{-1}, D= 0.042cm) in this study). Then the objective function is defined as

$$\Phi = \sum_s \sum_d \frac{\left[\left(\frac{M^{pert(t)}_{s,d}}{M^{ref}_{s,d}} P_{s,d}(\xi_0)\right) - P_{s,d}(\xi_n)\right]^2}{\left(\frac{M^{pert(t)}_{s,d}}{M^{ref}_{s,d}} P_{s,d}(\xi_0)\right)^2}$$

where M^{pert} = state obtained during perturbation
M^{ref} = predetermined reference state
$P_{s,d}$ = predicted detector readings obtained from initial distribution of optical properties ξ_0 = (μ_{a0} , D_0)

This objective function looks like the mean square error, but since the optical properties cannot be determined directly, the difference data is used. $P_{s,d}$ is obtained from the forward model ie. by finite element solver, and put into the objective function. Then this objective function is solved iteratively by the conjugate gradient descent algorithm that minimizes the objective function. In this study, the calculation of the gradient was performed using the adjoint differentiation technique.

In this study, markers are placed on the head to determine the 3D coordinates of the surface of the forehead as in figure 25. Then these 15 markers are removed and the whole head is marked according to the marks caused by the pressure of the markers. After all the markers are placed, the head is photographed from several angles to determine the 3D coordinates of all referenced points. And the surface of the forehead is approximated as a smooth contour by connecting the markers with B spline curves. Having generated the surface coordinates of the human forehead, the boundary of the domain, the corresponding volume is generated by a volumetric mesh generator.

Figure 26: Commercial instrument

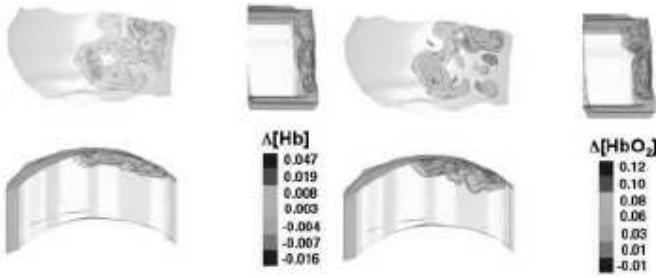

Figure 27: Δ[Hb] and Δ [HbO_2] images ([20])

The calculated $\Delta\mu_a$ values are the changes in the absorption coefficients at each node of the mesh. From these values, changes in oxyhemoglobin and deoxyhemoglobin concentrations are calculated from the equation

$$\Delta\mu_a^{\lambda} = \varepsilon_{HbO_2}^{\lambda}\Delta[HbO_2] + \varepsilon_{Hb}^{\lambda}\Delta[Hb]$$

where λ is the wavelength and ε_{Hb} and ε_{HbO2} are the known extinction coefficients for deoxyhemoglobin and oxyhemoglobin at the given wavelengths. Solving this equation at different wavelengths, one can find the concentrations to be

$$\Delta[Hb]_{meas} = \frac{\varepsilon_{HbO_2}^{\lambda_2}\Delta\mu_a^{\lambda_1} - \varepsilon_{HbO_2}^{\lambda_1}\Delta\mu_a^{\lambda_2}}{\varepsilon_{Hb}^{\lambda_1}\varepsilon_{HbO_2}^{\lambda_2} - \varepsilon_{Hb}^{\lambda_2}\varepsilon_{HbO_2}^{\lambda_1}},$$

$$\Delta[HbO_2]_{meas} = \frac{\varepsilon_{Hb}^{\lambda_1}\Delta\mu_a^{\lambda_2} - \varepsilon_{Hb}^{\lambda_2}\Delta\mu_a^{\lambda_1}}{\varepsilon_{Hb}^{\lambda_1}\varepsilon_{HbO_2}^{\lambda_2} - \varepsilon_{Hb}^{\lambda_2}\varepsilon_{HbO_2}^{\lambda_1}}.$$

Finally, these concentrations are combined for all source/detector combinations and a volumetric reconstruction is performed resulting in figure 26.

4) Joint Imaging:

Rheumatoid arthritis (RA) is a chronic, progressive, inflammatory disease, which primarily attacks peripheral joints and surrounding tendons and ligament [22]. Optical techniques have been shown to provide a new approach to early detection and monitoring of joint inflammation in patients with RA.

The studies by Hielscher *et. al.* [21][22] follow the same mathematical procedures as described in the 3D human hemodynamics measurements. However, in studies involving small tissue volumes, as well as in areas where the tissue contains low scattering regions like CSF in the brain, diffusion approximation has been found to have limited applicability. Therefore in such applications, transport equation is preferred for modeling.

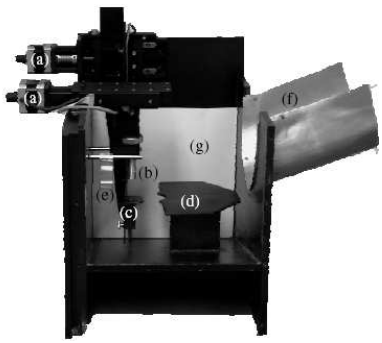

Figure 27 shows the system to image the fingers. And figure 28 is the results of the optical tomography imaging applied to joints.

Figure 28: The system to image the fingers ([22])

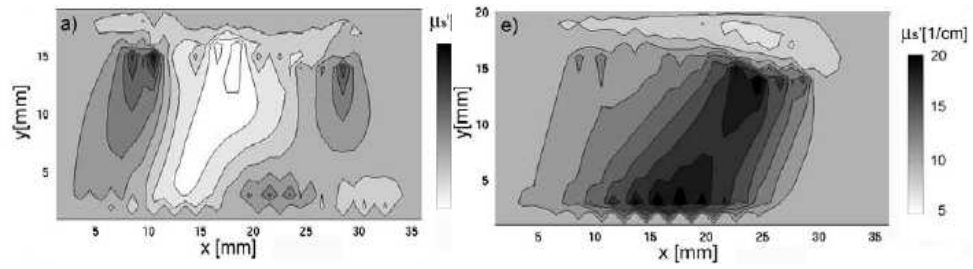

Figure 29 : Reconstructed cross sections of the scattering coefficient for two different fingers with the joint cavity located in the center a) not affected by RA b) affected by RA ([22])

FLUORESCENCE OPTICAL DIFFUSION TOMOGRAPHY (FODT)

Fluorescent ODT imaging is a relatively new imaging modality that combines the methodologies of ODT and fluorescent imaging. FODT has the advantage of using the deep tissue imaging capability of ODT and the high contrast and specificity properties of fluorescent dye tagging. The injected fluorophere may accumulate in diseased tissue because of increased blood flow as in cancer. Or it may have different decay properties in the diseased tissue independent of fluorophore concentration. In addition, contrast between tumors and surrounding tissue may be substantially improved by use of diagnostic agents that selectively target receptors specific to cancer cells [13]. A figure of the basic FODT scheme is given in figure 30.

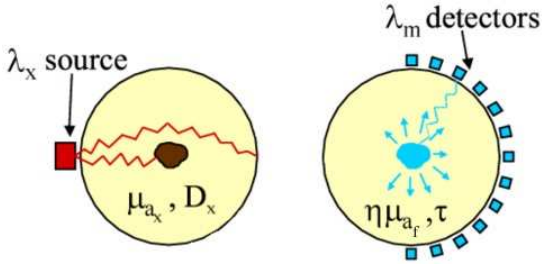

Figure 30: FODT, scattering and absorbtion in tissue ([23])

ODT reconstruction methods also apply for the FODT problem with some modifications. In FODT, two diffusion equations are used to model the propagation of modulated light through the tissue containing a fluorescent dye. One equation describes the absorption and scattering of photons at the excitation wavelength as in the case of ODT, while the other equation describes the fluorescent emission, followed by the absorption and scattering of the emitted light[23].

As in the case of ODT, FODT has time domain and frequency domain solutions. "In frequency-domain fluorescence ODT, sinusoidally modulated light wavelength is launched into the tissue. The excited fluorophore, when decaying to the ground state, emits light at a longer emission wavelength, and this emission is measured by an array of detection devices. These emission data are then used to perform a volumetric reconstruction of the yield (a measure of the fluorescence efficiency) and the lifetime (the fluorescent decay parameter)."[24]

The transport equation of modulated light in a fluorescent, highly scattering medium can be modeled using coupled diffusion equations:

$$\nabla \cdot [D_x(r)\nabla\phi_x(r,\omega)] - [\mu_{a_x}(r) + j\omega/c]\,\phi_x(r,\omega) = -S_x(r,\omega) \qquad (1)$$

$$\nabla \cdot [D_m(r)\nabla\phi_m(r,\omega)] - [\mu_{a_m}(r) + j\omega/c]\,\phi_m(r,\omega) = -\phi_x(r,\omega)\gamma(r,\omega)[1 - j\omega\tau(r)] \qquad (2)$$

$$\gamma(r,\omega) = \eta\mu_{a_{x\to m}}(r)\frac{1}{1 + [\omega\tau(r)]^2} \qquad (3)$$

x,m: excitation (λ_x) and emission (λ_m) wavelengths
$\phi(r,w)$: photon fluence (complex modulation envelope of the photon flux)
$S_x(r,w)$: excitation source distribution
Optical parameters → D(r): diffusion coefficient, $\mu_a(r)$: absorption coefficient
Fluorescence parameters → $\tau(r)$: lifetime, $\eta\mu_a(r)$:yield

In this formulation, the unknown parameters are $\mu_{ax}(r)$, $\mu_{am}(r)$,D_x, D_m, τ and $\eta\mu_a$. Reconstruction of these unknown parameters is obtained by three measurements at different wavelengths. Reconstructions of D_x and μ_{ax} are obtained using data from sources and detection at the excitation
Similarly, D_m and μ_{am} are obtained using data at the emission wavelength. Finally, having found these parameters, use of sources at the excitation λ_x and detectors filtered at λ_x will yield the fluorescence parameters [24]. A figure explaining these measurements is given below.

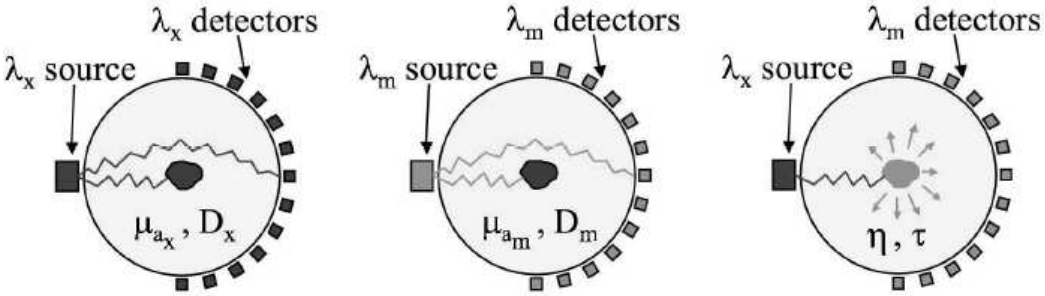

Source λ	Detector λ	Unknown Image	Observation
λ_x	λ_x	$x_x = [D_x, \mu_x]$	y_x
λ_m	λ_m	$x_m = [D_m, \mu_m]$	y_m
λ_x	λ_m	$x_f = [\eta, \tau]$	y_f

Figure 31: FODT measurement approach ([5])

Bayesian approach for the inverse problem:

Because the methods that linearize the forward model have limited accuracy, Milstein *et al.* offer nonlinear inversion methods such as the Bayesian approach. After discretizing the domain into N voxels, the unknown parameters are regarded as three image vectors. Then each image is formulated as a Bayesian inverse problem and the maximum a posteriori estimate is computed. x denoting one of the images and y denoting the corresponding observation, the maximum a posteriori estimate is given by

$$\hat{\mathbf{x}} = \arg\max_{\mathbf{x}\geq 0}\{\ \log p(\mathbf{y}|\mathbf{x}) + \log p(\mathbf{x})\ \}$$

p(y|x): data likelihood
p(x): prior density for the image.

The data likelihood is formed using a Gaussian Model

$$p(\mathbf{y}|\mathbf{x}) = \frac{1}{(\pi\alpha)^P|\Lambda|^{-1}}\exp\left[-\frac{\|\mathbf{y}-\mathbf{f}(\mathbf{x})\|^2_\Lambda}{\alpha}\right]$$

where P is the number of measurements, f is the appropriate forward operator and α is a scalar parameter for noise variance. For an arbitrary vector **w**, $\|w\|^2_\Lambda = w^H \Lambda w$ where H is the Hermitian transpose and $(\alpha/2)\Lambda^{-1}$ is the covariance matrix.

The prior density p(x) is modeled with Generalized Markov Random Fields given by

$$p(\mathbf{x}) = \frac{1}{\sigma^N z(p)}\exp\left[-\frac{1}{p\sigma^p}\sum_{\{i,j\}\in\mathcal{N}} b_{i-j}|x_i - x_j|^p\right]$$

x_i: image node values
N: dimension of the image vector
σ: normalization parameter
p: control parameter for the sharpness of the edge transition.

This Bayesian formulation allows the incorporation of a priori information and it encapsulates all available information about the problem model into an objective function to be optimized.

With the above information, reconstruction of the unknowns can be achieved by forming and optimizing three cost functions

$$\hat{\mu_{\mathbf{a}_x}} = \arg\min_{\mu_{\mathbf{a}_x}\geq 0,\alpha_{x,x}}\left\{\frac{1}{\alpha_{x,x}}||\mathbf{y}_{x,x} - \mathbf{f}_{x,x}(\mu_{a_x})||^2_{\Lambda_{x,x}} + \frac{1}{p_{\mu_{a_x}}\sigma^{p_{\mu_{a_x}}}_{\mu_{a_x}}}\sum_{\{i,j\}\in\mathcal{N}_{\mu_{a_x}}} b_{i-j}|x_i - x_j|^{p_{\mu_{a_x}}}\right\}$$

$$\hat{\mu_{\mathbf{a}_m}} = \arg\min_{\mu_{\mathbf{a}_m}\geq 0,\alpha_{m,m}}\left\{\frac{1}{\alpha_{m,m}}||\mathbf{y}_{m,m} - \mathbf{f}_{m,m}(\mu_{a_m})||^2_{\Lambda_{m,m}} + \frac{1}{p_{\mu_{a_m}}\sigma^{p_{\mu_{a_m}}}_{\mu_{a_m}}}\sum_{\{i,j\}\in\mathcal{N}_{\mu_{a_m}}} b_{i-j}|x_i - x_j|^{p_{\mu_{a_m}}}\right\}$$

$$[\hat{\gamma},\hat{\tau}] = \arg \min_{\gamma,\tau \geq 0, \alpha_{x,m}} \left\{ \frac{1}{\alpha_{x,m}} \|\mathbf{y}_{x,m} - \mathbf{f}_{x,m}(\gamma,\tau)\|^2_{\Lambda_{x,m}} + \frac{1}{p_\gamma \sigma_\gamma^{p_\gamma}} \sum_{\{i,j\}\in\mathcal{N}_\gamma} b_{i-j}|x_i - x_j|^{p_\gamma} + \frac{1}{p_\tau \sigma_\tau^{p_\tau}} \sum_{\{i,j\}\in\mathcal{N}_\tau} b_{i-j}|x_i - x_j|^{p_\tau} \right\}$$

where the subscripts (x,x), (m,m) and (x,m) specify the use of excitation or emission wavelength in the sources and detectors, f is the forward operator, Λ is the inverse covariance operator. This optimization can be performed using the iterative coordinate descent (ICD) algorithm.

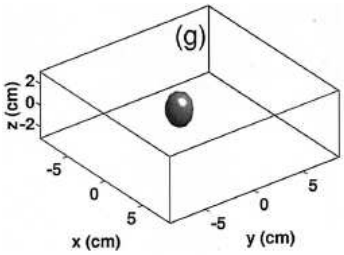

The setup used in studies [24][13][24] is given below with the results to give an idea about the experimental process[23].

Figure 32: True phantom with $\eta\mu_{af}$ =0.01 cm-1 ([13])

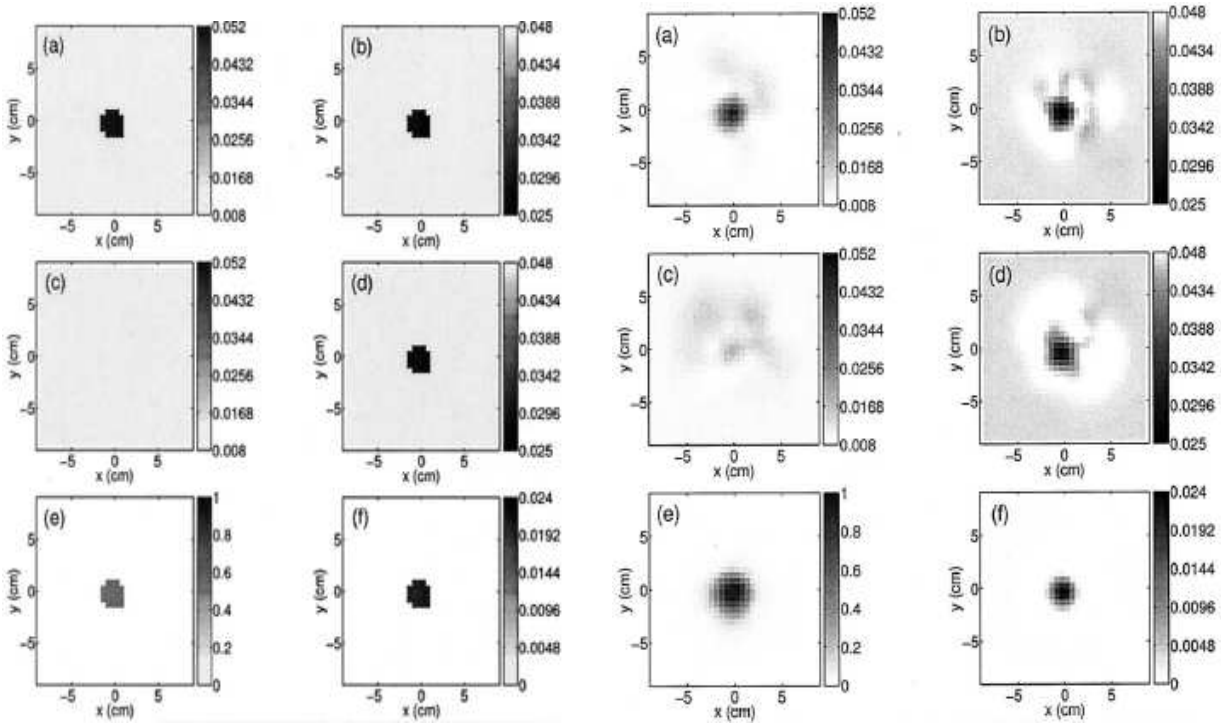

Figure 33: First two columns is the true phantom and second two columns is the reconstructed image a) μ_{ax} is in cm-1, b) Dx is in cm, c)μ_{am} is in cm-1, d)D_m is in cm, e) τ is in ns, f) $\eta\mu_{af}$ is in cm-1 ([13])

Reconstruction of Kinetic Parameters:

In the above studies, the time varying properties of the fluorescent yield $\eta(r,t)$ was not taken into account. However, organs such as liver and kidney tend to clear the fluorescent agent out of the blood pool. Milstein et al.[25] tries to solve this problem by applying compartmental models. "In a compartmental model, the body consists of a number of compartments, conceptual regions where the drug's concentration is assumed to be uniform. A system of differential equations given below describes the exchange of the drug among different compartments. Let κ_T and κ be the rate constants for entering and leaving the tissue, respectively, and let κ_O be the rate constant for removal of the fluorescent dye from the blood due to the kidney, liver, or other means."[25] Then the concentrations are obtained by solving

$$\begin{aligned} \frac{dc_B}{dt} &= -\kappa_B c_B + \kappa c_T \\ \frac{dc_T}{dt} &= \kappa_T c_B - \kappa c_T \end{aligned}$$

where $\kappa_B = \kappa_T + \kappa_O$

The experimentally observed fluorescent yield, which is proportional to the concentration of fluorophore, is some weighted sum of the tissue and blood compartments:

$$\eta(r,t) \simeq a_1(r)c_T(r,t) + a_2(r)c_B(r,t).$$

Assume that at injection time $t = 0$, $c_B = c_{B0}$ and $c_T = 0$.
Solving the differential equation and substituting into the previous equation yields a solution of the form:

$$\eta(r,t) = \gamma_1(r)\exp[-\gamma_4(r)t] - \gamma_2(r)\exp[-\gamma_3(r)t].$$

Since the five parameters $a1(r)$, $a2(r)$, $\kappa(r)$, $\kappa B(r)$, and κT (r) are not uniquely recoverable, the biexponential model parameters $\gamma 1(r)$, $\gamma 2(r)$, $\gamma 3(r)$, and $\gamma 4(r)$ are calculated to reconstruct η(r,t). More information about these solutions can be found in [25].

FODT APPLICATIONS:

The FODT studies given above all depended on some simulations of the tissue. The optical characteristics of tissue and tumors were imitated by some solutions. In this section, two experiments on mice will be given.

In the study by Sevick-Muracca [26] with the system shown in figure 34, a tumor bearing mouse is injected with Fluorophore Cy5.5 dye and fluorescent intensity decrease is calculated. 48 hours later the mouse is imaged and the result is as given in figure 35.

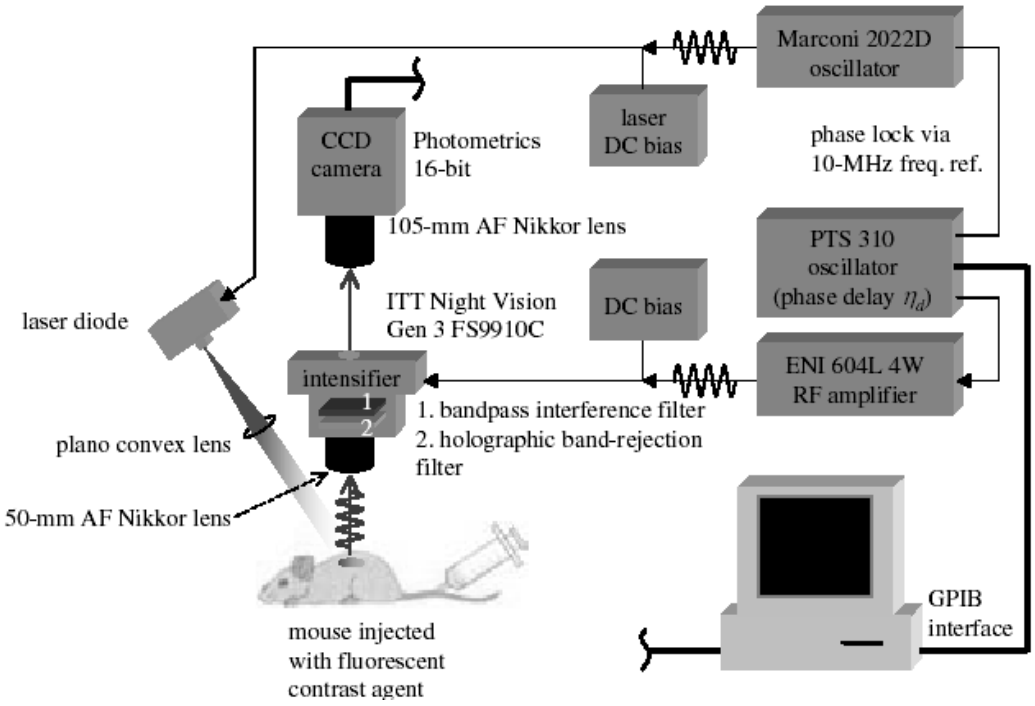

Figure 34: White light and fluorescent image of animal 48 hours after 1 nmol administraion of CY5.5-EGF ([26])

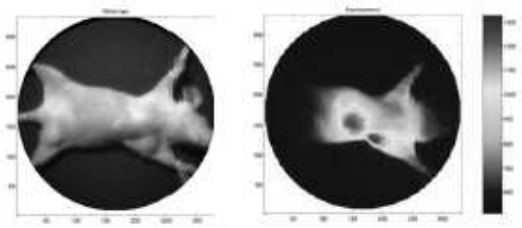

Figure 35: Schematic of animal imaging system ([26])

In figure 35, the bright spot in the center of the animal arises due to the EGFr rich liver and the bright spot to the right is the tumor known to express the EGF receptor.

A similar study is given by Lesage where the mouse is injected by Fluorophore Cy5.5 by a cubical inclusion thorough a small skin incision. The animal already has fluorescence originating from the food. This study makes the discrimination by these sources and the 3D reconstruction results are as seen in figure 36.

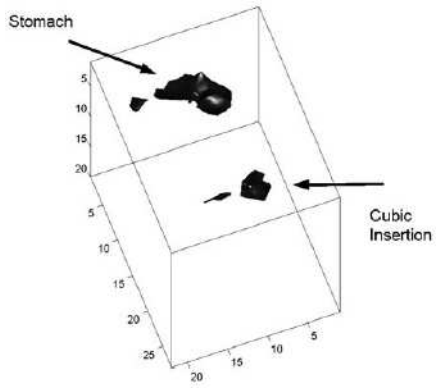

Figure 36: 3D Reconstruction of the mouse scan with the inclusion ([27])

These studies are important because the application of some drugs for tumor treatment depends on the presence of some molecular markers. Diagnostic imaging of these markers with FODT would provide a criterion for the selection of appropriate molecular therapy for individual patients.

CONCLUSION

Various techniques used in optical imaging has been discussed and a wide variety of methods has been introduced throughout this report for the ODT and FODT problems. However, for the case of ODT and FODT, due to the nonlinear nature of the forward problem, the methods are still not powerful enough. Radiative transfer equations offer a better model for photon propagation than diffusion equations but they are much more expensive computationally (takes several hours on a general PC). On the other hand, the diffusion equation is just an approximation to this model and its applicability is limited to highly scattering media. However, although biological tissues are highly scattering, still they are heterogeneous and may contain regions that are highly absorbing or low scattering. Even with the diffusion equation, a forward model would still take too much time for 3D geometries and the inverse problem is always ill-posed and may lead to divergent results. Besides, most of these methods have been performed in unrealistic physical conditions and geometries.

Therefore, there is still too much work to be done before the full potential of optical tomography can be realized, but the benefits are worth the effort!

References

[1] M. S. Schießl, "Blind Signal Separation from Optical Imaging Recordings with Extended Spatial Decorrelation," IEEE Transactions On Biomedical Engineering, Vol. 47, No. 5, May 2000 573

[2] http://oilab.tamu.edu/, Texas A&M University Optical Imaging Laboratory

[3] Biomedical optics research laboratory, University College, UK , Available: http://www.medphys.ucl.ac.uk/research/borl/ , July 20, 2004 [date accessed]

[4] http://www.chem.vt.edu/chem-ed/crossref/ac-spectroscopy.html

[5] C. A. Bouman, K. J. Webb, "Biomedical Optical Imaging Tutorial 1," IEEE International Symposium on Biomedical Imaging, Washington DC, April 15, 2004.

[6] J. C. Hebden, A. Gibson, T. Austin *et al.*, "Imaging changes in blood volume and oxygenation in the newborn infant brain using three-dimensional optical tomography", Physics in Medicine and Biology, 49 (2004) 1117–1130

[7] Principle of Optical Topography System. [Online]. Available: http://www.hitachi-medical.co.jp/how_to/opt-e/genri-top.html, July 18, 2004 [date accessed].

[8] G. Taga, K. Asakawa, A. Maki *et al.*, "Brain imaging in awake infants by near-infrared optical topography," Proceedings of the National Academy of Sciences of U S A, 100(19):10722-7. Epub 2003 Sep 05.

[9] K. K. Chu, "Use of Optical Coherence Tomography for the Imaging of Cortical Tissue," Duke University July 27, 2001

[10] "Optical Coherence Tomography for Diagnosing Retinal Disease", Alberta Heritage Foundation for Medical Research Technote, Tn, 41 August 2003

[11] H. Schlossberg, "Optical Coherence Tomography, Air Force Office of Scientific Research," [Online] Available : http://www.afrlhorizons.com/Briefs/Mar03/OSR0209.html , July 18, 2004 [date accessed]

[12] Eye Clinic of Optical Coherence Tomography, New England Eye Center. [Online]. Available : http://www.nexus.com.cn/products/idb/html%20for%20each%20modality/images/Optical%20Coherence%20Tomography_image.html, July 18, 2004 [date accessed]

[13] A. B. Milstein, S. Oh, KJ Webb, CA Bouman, Q. Zhang, DA Boas, RP Millane, "Fluorescence optical diffusion tomography," Appl Opt 42, 3081—3094 (2003).

[14] D.A. Boas, D.H. Brooks, E.L. Miller, C.A. DiMarzio , M. Kilmer, R.J. Gaudette and Q. Zhang, "Imaging the body with diffuse optical tomography." IEEE Signal Processing Magazine 18(6): 57-75 (2001).

[15] S. R. Arridge and J.C. Hebden, "Optical Imaging in Medicine: II. Modeling and Reconstruction", Phys. Med. Biol. 42 , p 841-853, 1997

[16] K. Tahir. (1997, May) Optical Tomography. Applied Optics Group, Imperial College, London. [online] Available : http://op.ph.ic.ac.uk/tomog/tomog.html, July 18, 2004 [date accessed]

[17] S. R. Arridge, "Time Domain Optical Tomography," ISBI 2004: 1486-1489

[18] B. W. Pogue, M. Testorf, T. McBride, U. Osterberg, K. Paulsen, "Instrumentation and design of a frequency-domain diffuse optical tomography imager for breast cancer screening," Optics Express, 1(13), 394-403 (1997).

[19] A. M. Siegel, J. P. Culver, J. B. Mandeville, and D. A. Boas, "Temporal comparison of functional brain imaging with diffuse optical tomography and fMRI during rat forepaw stimulation," Phys. Med. Biol., vol. 48, no. 10, pp. 1391-1403, May 21 2003

[20] A.Y. Bluestone, G. Abdoulaev, C. Schmitz, R.L. Barbour, A.H. Hielscher , "Three-dimensional optical-tomography of hemodynamics in the human head", *Optics Express* 9(6), pp. 272-286, 2001. (http://www.opticsexpress.org/abstract.cfm?URI=OPEX-9-6-272)

[21] A.H. Hielscher, G. Abdoulaev, A. Klose, A. Bluestone, J. Lasker, "Near infrared optical tomographic imaging of fluid containing tissues," Biomedical Imaging Proceedings, p.70 – 73, July 2002.

[22] A. Hielscher, A. D. Klose, A. Bluestone, J. M. Lasker, B. Moa-Anderson, J. M. Masciotti, G. Abdoulaev, A. Scheel, M. Stewart, U. Netz, J. Beuthan, "Optical Tomographic Imaging of Small Tissue Volumes: From Rat Brains to Human Finger Joints," ISBI 2004: 1467-1470

[23] A. B. Milstein, Imaging of Absorption, Scattering, and Fluorescence in Diffuse Media, available: http://shay.ecn.purdue.edu/~amilstei/odt/odt.html, May 24, 2004 [date accessed]

[24] A. B. Milstein, Q. Zhang, S. Oh, K.J. Webb, C.A. Bouman, R.R. Millane, D.A. Boas, "Fluorescence imaging in optical diffusion tomography," IEEE Proc. on Biomedical Imaging, pp 58- 6, 2002

[25] A. B. Milstein, S. Oh, K. J. Webb, C. A. Bouman, "Direct Reconstruction of Kinetic Parameter Images in Fluorescence Optical Diffusion Tomography." ISBI 2004: 1107-1110

[26] E. M. Sevick-Muraca, "Fluorescence-Enhanced Optical Imaging and Tomography for Cancer Diagnostics." ISBI 2004: 1482-1485

[27] F. Lesage, A.Belenkov, "In vivo lifetime discrimination using time domain fluorescence imaging," ISBI 2004: 688-691

APPENDIX

ELECTROMAGNETIC SPECTRUM

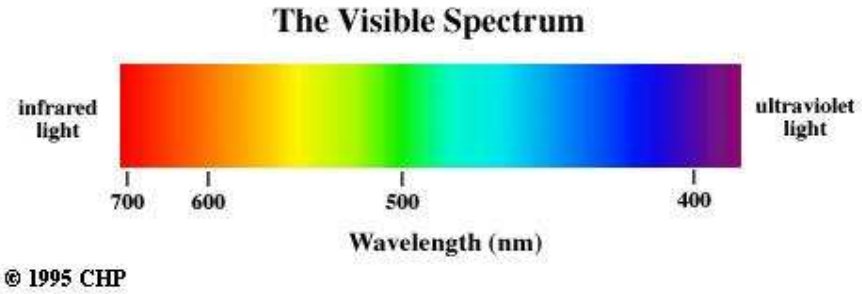

Type of Radiation	Frequency Range (Hz)	Wavelength Range	Type of Transition
gamma-rays	10^{20}-10^{24}	<1 pm	nuclear
X-rays	10^{17}-10^{20}	1 nm-1 pm	inner electron
ultraviolet	10^{15}-10^{17}	400 nm-1 nm	outer electron
visible	4-7.5x10^{14}	750 nm-400 nm	outer electron
near-infrared	1x10^{14}-4x10^{14}	2.5 µm-750 nm	outer electron molecular vibrations
infrared	10^{13}-10^{14}	25 µm-2.5 µm	molecular vibrations
microwaves	3x10^{11}-10^{13}	1 mm-25 µm	molecular rotations, electron spin flips*
radio waves	<3x10^{11}	>1 mm	nuclear spin flips*

Optical Tomography Groups

- Randall L. Barbour - SUNY Downstate Medical Center
- A.H. Hielscher, Dept. of Biomedical Eng. And Radiology, Columbia Univ.
- Charles A. Bouman, Purdue Univ.
- Huabei Jiang - Clemson University
- Optical Imaging and Spectroscopy at UPENN
- Arjun Yodh - Optical Imaging and Spectroscopy, University of Pennsylvania
- David Boas - MGH
- Eva Sevick-Muraca – Texas A&M University
- Simone Arridge - University College London
- MONSTIR Download
- Philips Optical Mammography
- Optical Tomography, RWTH Aachen, Germany
- University of Hertfordshire, UK
- Photon Migration, University of Illinois
- Electro-Optics Technology, Tufts University

Biomedical Optics Groups

- Beckman Laser Institute
- MGH Laser Center
- Steven Jacques - Oregon Medical Laser Center
- Applied Optics Group: University of Edinburgh
- Applied Optics Group: University of L'Aquila
- Applied Optics Lab: University of New Mexico
- Applied Optics Group: Imperial College
- Optical Imaging Laboratory: UCLA
- Laboratory for Fluroescence Dynamics: UIUC.